ResearchGate

See discussions, stats, and author profiles for this publication at: https://www.researchgate.net/publication/343260853

PROBA-3 mission and the Shadow Position Sensors: Metrology measurement concept and budget

Article *in* Advances in Space Research · July 2020

DOI: 10.1016/j.asr.2020.07.022

CITATIONS
3

READS
194

27 authors, including:

Davide Loreggia
National Institute of Astrophysics
97 PUBLICATIONS **7,805** CITATIONS

SEE PROFILE

Silvano Fineschi
National Institute of Astrophysics
350 PUBLICATIONS **4,905** CITATIONS

SEE PROFILE

Alessandro Bemporad
National Institute of Astrophysics
207 PUBLICATIONS **2,247** CITATIONS

SEE PROFILE

Marta Casti
National Institute of Astrophysics
47 PUBLICATIONS **154** CITATIONS

SEE PROFILE

Some of the authors of this publication are also working on these related projects:

Postdoc View project

"Cataclysmic Variables and Related Objects" View project

All content following this page was uploaded by Silvano Fineschi on 10 January 2021.

The user has requested enhancement of the downloaded file.

Available online at www.sciencedirect.com

ScienceDirect

Advances in Space Research xxx (xxxx) xxx

ADVANCES IN SPACE RESEARCH (a COSPAR publication)

www.elsevier.com/locate/asr

PROBA-3 mission and the Shadow Position Sensors: Metrology measurement concept and budget

Davide Loreggia [a,*], Silvano Fineschi [a], Gerardo Capobianco [a], Alessandro Bemporad [a], Marta Casti [a,j], Federico Landini [a], Gianalfredo Nicolini [a], Luca Zangrilli [a], Giuseppe Massone [a], Vladimiro Noce [b], Marco Romoli [c], Luca Terenzi [d], Gianluca Morgante [d], Massimiliano Belluso [e], Cedric Thizy [f], Camille Galy [f], Aline Hermans [f], Pierre Franco [f], Ariane Pirard [f], Laurence Rossi [f], Steve Buckley [g], Raymond Spillane [g], Martin O'Shea [g], Damien Galano [h], Jorg Versluys [h], Ken Hernan [h], Luciano Accatino [i]

[a] *INAF-Astrophysical Observatory of Turin, Via Osservatorio, 20, 10025 Pino Torinese, Turin, Italy*
[b] *INAF-Astrophysical Observatory of Arcetri, Largo E. Fermi, 5, 50125 Florence, Italy*
[c] *University of Florence, Department of Astronomy, Via Sansone 1, 50019 Florence, Italy*
[d] *INAF-Astrophysical Observatory of Bologna, Via Piero Gobetti, 93/3, 40129 Bologna, Italy*
[e] *INAF-Astrophysical Observatory of Catania, Via S.Sofia, 78, 95123 Catania, Italy*
[f] *Centre Spatial de Liege, Av. du Pre Aily, 4031 Liege, Belgium*
[g] *ON Semiconductor Building 6800, Avenue 6000 Cork Airport Business Park, Cork T12 CDF7, Ireland*
[h] *European Space Agency, Keplerlaan 1, 2201 AZ Noordwijk, the Netherlands*
[i] *Ac-Consulting, Via Trieste, 16/B, 10098 Rivoli, Turin, Italy*
[j] *ALTEC S.p.A., Corso Marche, 79, 10146 Torino TO, Italy*

Received 24 January 2020; received in revised form 13 July 2020; accepted 16 July 2020

Abstract

PROBA-3 is a space mission of the European Space Agency that will test, and validate metrology and control systems for autonomous formation flying of two independent satellites. PROBA-3 will operate in a High Elliptic Orbit and when approaching the apogee at $6{\cdot}10^4$ Km, the two spacecraft will align to realize a giant externally occulted coronagraph named ASPIICS, with the telescope on one satellite and the external occulter on the other one, at inter-satellite distance of 144.3 m. The formation will be maintained over 6 hrs across the apogee transit and during this time different validation operations will be performed to confirm the effectiveness of the formation flying metrology concept, the metrology control systems and algorithms, and the spacecraft manoeuvring. The observation of the Sun's Corona in the field of view $[1.08;3.0]R_{Sun}$ will represent the scientific tool to confirm the formation flying alignment. In this paper, we review the mission concept and we describe the Shadow Position Sensors (SPS), one of the metrological systems designed to provide high accuracy (sub-millimetre level) absolute and relative alignment measurement of the formation flying. The metrology algorithm developed to convert the SPS measurements in lateral and longitudinal movement estimation is also described and the measurement budget summarized.
© 2020 COSPAR. Published by Elsevier Ltd. All rights reserved.

Keywords: Space mission; Formation flying; Coronagraph; Satellite constellation; Solar physics; High accuracy metrology

* Corresponding author.
E-mail address: davide.loreggia@inaf.it (D. Loreggia).

https://doi.org/10.1016/j.asr.2020.07.022
0273-1177/© 2020 COSPAR. Published by Elsevier Ltd. All rights reserved.

Please cite this article as: D. Loreggia, S. Fineschi, G. Capobianco et al., PROBA-3 mission and the Shadow Position Sensors: Metrology measurement concept and budget, Advances in Space Research, https://doi.org/10.1016/j.asr.2020.07.022

1. Introduction

Formation flying (FF) of multiple spacecraft gathers great interest from the scientific community due to the opportunity to significantly improve the observation capabilities and resolution limits. From the last decades of the last century, numerous mission concepts, based on multi spacecraft constellation and formation flying, have been proposed to satisfy a large diversity of scientific objectives. Even if many of them have been abandoned, mainly due to the large gap between the required and the available technology, and the cost, starting the new millennium the idea to concretize these concepts have become more then realistic and many agencies have proposed or made in operation space missions based on a formation-flying concept [Leitner, 2004, Xiang and Jorgensen, 2005].

Gathering experience from mission such us CLUSTER [Escoubet et al., 1997], GRACE [Tapley et al., 2004], and Cosmo-SkyMed [Covello et al., 2008], composed of two or more spacecraft in similar orbits with no active or semi-automatic control, the employment of multiple satellites in a variable configuration confirmed how these new mission architectures enable unprecedented science performance. The step forward to realize high performing formation flying is to make effective a multi-spacecraft configuration using an active control scheme to autonomously realize and maintain the absolute and relative positioning (real-time and closed-loop control systems).

The FF concept was studied for many applications such as earth observation, astrometry, interferometry, and coronagraphy. In this sense, the TerraSAR-X/TanDEM-X mission [Krieger et al., 2007, Werninghaus, 2004] represented the first space mission equipped and operated routinely with an autonomous formation flying system. Mission like Darwin [Wallner et al., 2006], TPF [Blackwood et al., 2003] LISA [Jennrich, 2004] have been thought as accurate interferometers able to materialize large/huge baselines with multiple collecting apertures maintained in interferometric configuration over long periods. Similarly, PROBA-3 [Landgraf and Mestreau-Garreaub, 2013] and StarShade [Glassman et al., 2009] are expected to trace a new frontier for solar and stellar coronagraphy, yielding to observe the Sun's Corona phenomena with high spatial resolution very close to the solar limb, and to permit to observe, for the first time, *exo*-planet close to their parent star, respectively.

With the great advantage of increased functionality and enhanced reliability, all these FF concepts share common features: they impose stringent constraints on the relative and absolute positioning, pointing, and stabilization of the spacecraft. This requires the design, the study, and the implementation of fine metrology techniques and actuation systems as well as the verification and validation of robust control algorithms. The in-flight testing of formation flying control techniques became mandatory and, in this sense, the PRISMA mission [Bodin et al., 2009], launched in 2010, represented the first demonstrator of in-orbit FF and rendezvous metrology. PRISMA was flown on a Low Elliptical Orbit and automatic acquisition of the FF was successfully tested through different experiment that used GPS control, Radio Frequency Link, and Visual Based Sensors. The achieved level of performance was below the requirements of future mission concepts since the equipment suite did not involve any fine actuation or adequate optical metrology and the gravity gradient environment was far from favourable. Therefore, a detailed approach to accurate modelling and validation of high accuracy metrology systems has become the driving goal for the next generation FF missions.

In this scenario, PROBA-3, "PRoject for On-Board Autonomy", represents a cornerstone mission aimed at realizing full automatic acquisition and maintenance of the FF of two independent spacecraft flying on a High Elliptical Orbit (HEO). PROBA-3 is a mission part of the ESA In-Orbit Demonstration (IOD) strategy, implemented by the Directorate of Technical and Quality management (D/TEC), supported by ESA's General Support Technology Programme, and it is dedicated to the verification and validation of precise formation flying metrology concept and manoeuvres, including formation acquisition, maintenance, resizing and retargeting.

To this end, different metrology instrumentations are implemented that will be operated to align the two spacecraft down to millimetre accuracy level. In the following sections 2 and 3, we review the PROBA-3 mission and the main metrology sub-systems. In the subsequent sections, we focus on the Shadow Position Sensors, the metrology subsystem that is expected to return the measurement of the absolute and relative positioning of the formation with the finest accuracy.

2. PROBA-3 mission

The PROBA-3 mission consists of two small spacecraft which will acquire and maintain a formation flying with relative position control accuracy that varies with the inter-satellite distance (ISD). PROBA-3 metrology concept will be tested to resize the formation between 25 m and 250 m, and to retargeting up to 30° (Fig. 1) with respect to the Sun direction, and with accuracy varying between 2 mm at 40 m, 5 mm at 150 m, and 8 mm at 250 m. This two bodies system will behave as a virtual rigid structure being commanded to rotate and to point at the desired direction.

The formation is realized over six hours long passage around the apogee, to maximize the advantage of the gravitational derivative and to minimize the overall power consumption budget. After this operation period, the formation breaks and the two satellites are positioned in a safety orbit to avoid collision and evaporation (Direct Transfer Manoeuvre 1- DTM1). Approaching the perigee, the GPS control drives the FF by controlling proper orbital parameters and by propagating the configuration through the new orbit. Arriving at the DTM2 point, the FF is re-acquired and operations repeat. In the following Fig. 2, a reproduction of the PROBA-3 orbit is given.

Please cite this article as: D. Loreggia, S. Fineschi, G. Capobianco et al., PROBA-3 mission and the Shadow Position Sensors: Metrology measurement concept and budget, Advances in Space Research, https://doi.org/10.1016/j.asr.2020.07.022

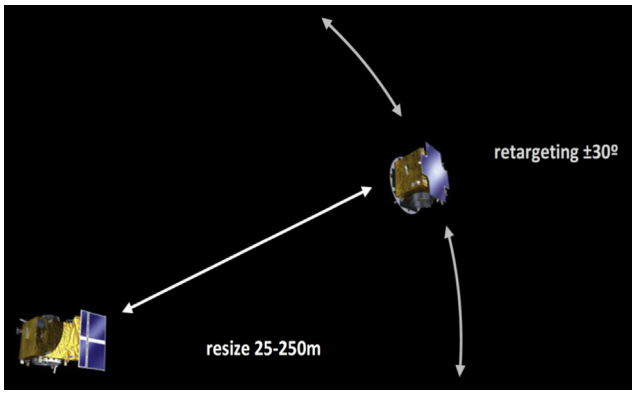

Fig. 1. PROBA-3 manoeuvring for metrology testing and validation.

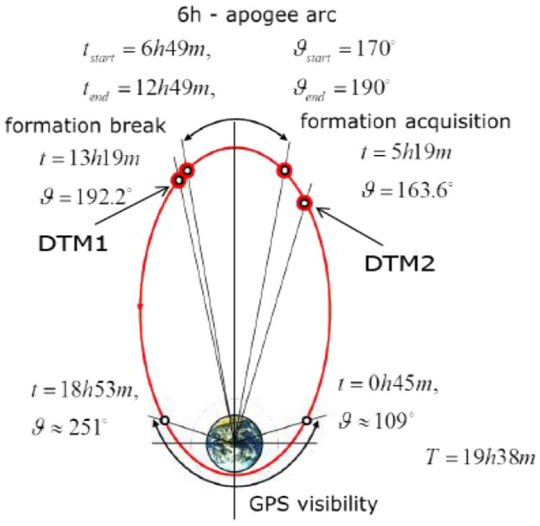

Fig. 2. PROBA-3 orbit details.

The scientific tool used for validating the formation flying is the observation of the Sun's Corona by realizing a diluted externally occulted coronagraph [Galy et al., 2015], named ASPIICS, "Association of Spacecraft for Polarimetric and Imaging Investigation of the Corona of the Sun", with the telescope on one spacecraft (Coronagraph SpaceCraft - CSC) and the occulter disk on the other one (Occulter SpaceCraft - OSC). Coronagraphic observations will be obtained when the two spacecraft will be in FF at a relative ISD = 144.3 m. This distance is an average value linked to the dimension of the apparent radius of the Sun, R_{Sun}, the radius of the occulter disk, R_{disk} = 710-mm, and the radius of the entrance pupil of the telescope, R_{pupil} = 25 mm, by the relation:

$$ISD = \frac{R_{disk} - R_{pupil}}{\tan(occ \cdot R_{Sun})} - \frac{T}{2} - R_{edge} \cdot \sin(R_{Sun})$$

T = 35 mm is the thickness of the occulter disc and R_{edge} is the radius of curvature of the disk edge. R_{Sun} varies during the mission and the ISD will change accordingly, as shown in Fig. 3, to have the same umbra and penumbra dimension on the pupil plane of the telescope. The factor *occ* = 1.02 is the reference *over-occultation* required to the external occulter in order to satisfy the mission scientific requirements [Zuckov, 2018, Galano et al., 2019].

The PROBA-3 observation configuration takes great advantage from the external occultation at so large ISD, combined with a customized toroidal geometry of the occulter [Baccani et al., 2016] that yields to a strong reduction of the stray light. This configuration is expected to return scientifically relevant high-resolution coronagraphic observations very close to the solar limb [Zuckov, 2018], in the field of view [1.08; 3.0]R_{Sun}, where the inner value 1.08 takes into account the extra internal occultation to remove residual stray light [Galy et al., 2015].

Thanks to a filter wheel mounted in front of the ASPIICS detector, observations will be performed over some reference waveband in un-polarised and polarised light conditions. In the following Table 1, the main observation tips are given.

At the end of the two years mission, PROBA-3 is expected to return in-orbit confirmation of different automatic metrology sub-systems and control algorithms, safety, repeatability, and rendezvous experiments in HEO.

3. Formation flying metrology and control

The FF will be acquired at subsequent steps, by operating different metrology sub-systems, summarized in Table 2, and implementing different metrology concepts, alignment, and control procedures, starting from a rough alignment (at cm level) to the finest obtainable (sub-millimetre level) [Contreras et al., 2017].

The two spacecraft are 3-axis stabilized using reaction wheels with the OSC being responsible for high accuracy actuation using cold gas milli-Newton thrusters, while the CSC performing main relative orbital maintenance impulsive manoeuvres with monopropellant thrusters. For attitude determination, a set of three optical heads from the

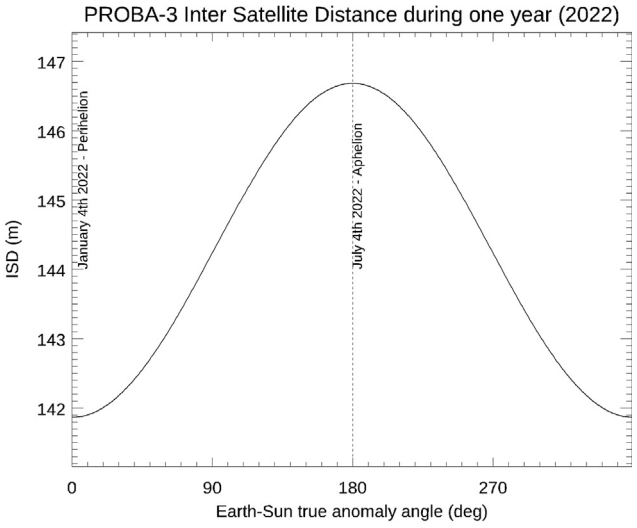

Fig. 3. PROBA-3 inter satellite distance (ISD) variation over one year.

Please cite this article as: D. Loreggia, S. Fineschi, G. Capobianco et al., PROBA-3 mission and the Shadow Position Sensors: Metrology measurement concept and budget, Advances in Space Research, https://doi.org/10.1016/j.asr.2020.07.022

Table 1
PROBA-3 observation tips.

Parameters	Values
Payload	2 independent satellites flying in formation
Instrument	Externally occulted coronagraph, optimised for the observation of the inner corona
Inter Satellite Distance	144.3 *m*
Pupil diameter	50 mm
Plate scale	2.8 arcsec / pixel
Field of view	[1.08, 3.00] solar radii
Detector	Full frame CCD, 2 K × 2 K, passively cooled
Exposure time	Adjustable in [1; 600] sec ensured by an electro-mechanical shutter
Wide wavelength range	Selected by a wide-band (WB) filter [540 : 590] nm
He I D3 line	By a selectable narrow-band filter @ 587.6 nm
Fe XIV line	By a selectable narrow-band filter @ 530.9 nm
Polarised light	3 polarisers (0°; ±60°) mounted over a WB filter
Imaging cadence	As high as 1 image / 2 s
Power Consumption	300 W (CSC), 180 W (OSC)

Table 2
PROBA-3 Formation flying metrology suite.

Item	On CSC	On OSC
Formation Flying units		
Occulter Position Sensor Emitters (OPSE)	Coronagraph detector	3x(+3x) LEDs
Fine Lateral and Longitudinal Sensors (FLLS)	1x corner cube (retroreflector)	Sensors and laser emitters
Shadow Position Sensors (SPS)	8x SiPM	Occulter (∅=1.4 m)
Visual based sensors	8x IR LEDS	Optical head (OH) + electronics
Inter satellite link systems	2x Rx-Tx + 2x antenna	2x Rx-Tx + 2x antenna
Actuators		
Propulsion Thrusters	2x 8x 1 N Monoprop.	2x 12x 10mN Cold Gas
Reaction Wheel	Pyramid of 4 units	/
GNC		
Star trackers	3x OH + 2x electronics	
Sun Sensors	5 (1 fine and 4 coarse) redundant cosine sensors	
Rate Sensors	2x units (3 axis)	
GPS	2x receivers + 2x antennas	

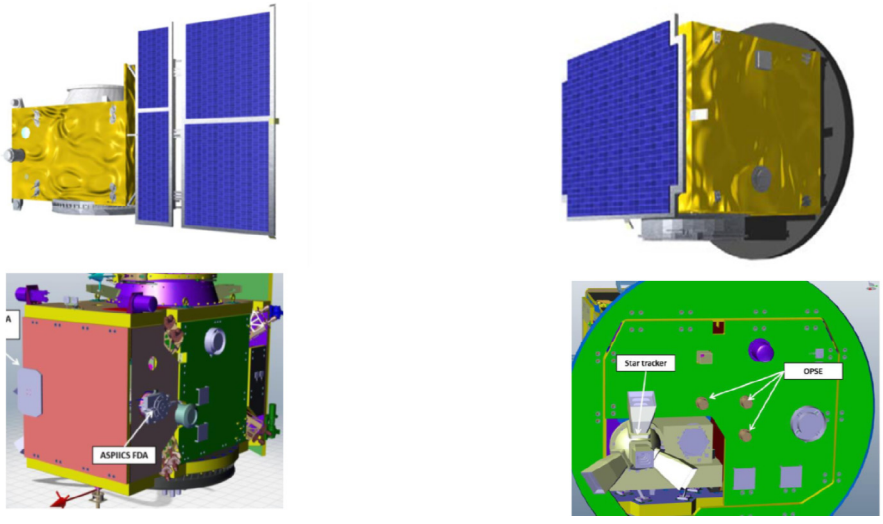

CSC : 300Kg ; 300W OSC: 230Kg ; 180W

Fig. 4. PROBA-3 satellites (courtesy of ESA): Coronagraph spacecraft (left): Occulter spacecraft (right).

Please cite this article as: D. Loreggia, S. Fineschi, G. Capobianco et al., PROBA-3 mission and the Shadow Position Sensors: Metrology measurement concept and budget, Advances in Space Research, https://doi.org/10.1016/j.asr.2020.07.022

star sensors (STR) will be used. Conventional Sun sensors and gyros will be used for safety (see Fig. 4).

The Fine Lateral and Longitudinal Sensor (FLLS) is the system that will permit to reach the final alignment. Once the FF configuration will be reached, the Shadow Position Sensors (SPS) will be operated to monitor the penumbra and to maintain the alignment by returning lateral position measurements with an expected accuracy of 0.5 mm. In the following Table 3, the schematized operation mode of the different metrology systems for navigation control and FF acquisition, is shown.

The metrology sensors return the position measurement to the On-board Guidance and Navigation Control (GNC) system and the navigation functions estimate the actual values of the attitude and of the relative position with respect to the expected values. Once determined the alignment correction, the controllers try to nullify the difference navigation–guidance, using the CSC and OSC reaction wheels and OSC cold gas thrusters. The navigation functions (at S/C and FF level) are based on Kalman filters as schemed in the following Fig. 5.

The FF approaching procedure and the alignment acquisition are shown in Fig. 6.

The final lateral position error is given by correlating the measurements from the FLLS with those from the SPS, and accounting for different contributions, such as constant bias (e.g., fixed misalignment between sensors), slow drift and variation (e.g., orbital and seasonal thermo-elastic change), high frequency random noise (e.g., sensor noise, micro-vibrations). In the end, the mission expected (lateral) positioning error is equal to 10 mm (3σ) with FLLS and with the SPS supporting for calibration, and of about 1–2 mm (3σ) with SPS in closed loop (assuming 0.5 mm error on the SPS measurements). The pointing error will be of about 15 arc-seconds (3σ) with large part being constant bias or slow varying bias (time constants > hours). The longitudinal and lateral errors are (to a very good approximation level) not correlated. Pointing and positioning error will be strictly dependent on the periodic in-flight calibration.

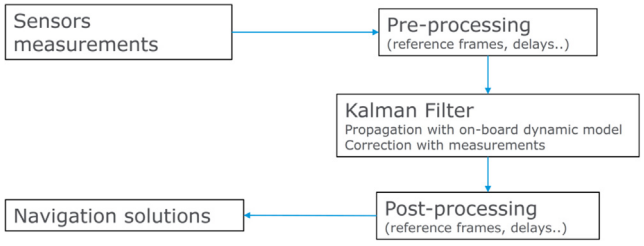

Fig. 5. PROBA-3 navigation control scheme (Courtesy of ESA).

4. Shadow Position Sensors

The Shadow Position Sensors (SPS) metrology subsystem consists of a series of 8x (3x3)mm^2 SiPM (Silicon PhotoMultiplier) assembled on a Printed Circuit Board (PCB), equally spaced along a circumference with diameter ∅ = 110 mm, and centred on the ASPIICS telescope's entrance aperture (∅ = 50 mm). As shown in Fig. 7, the PCB also hosts the SPS proximity electronics [Noce et al., 2019], and interfaces with the Coronagraph Control Box (CCB) by means of 2x 37pin connectors feeding the power and taking out the SiPM digitized irradiance measures to the on-board control software (OBSW).

Table 3
Metrology system operation for navigation control and alignment acquisition.

FLLS:
- Laser on one spacecraft;
- Retroreflector on the other spacecraft;
- High accuracy positioning;

Vision based System (VSB):
- Wide Angle Camera (WAC);
- Narrow Angle Camera (NAC);
- Light pattern on the other spacecraft;

Inter-Satellite Link (ISL):
- S-band radio frequency link between spacecraft
- Omni-directional;

Relative GPS navigation (rGPS):
- Integrated processing GPS raw;
- Measurements from both spacecraft.

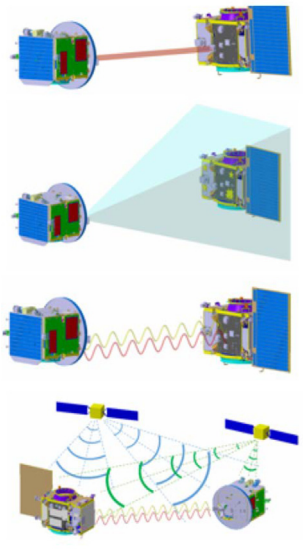

Please cite this article as: D. Loreggia, S. Fineschi, G. Capobianco et al., PROBA-3 mission and the Shadow Position Sensors: Metrology measurement concept and budget, Advances in Space Research, https://doi.org/10.1016/j.asr.2020.07.022

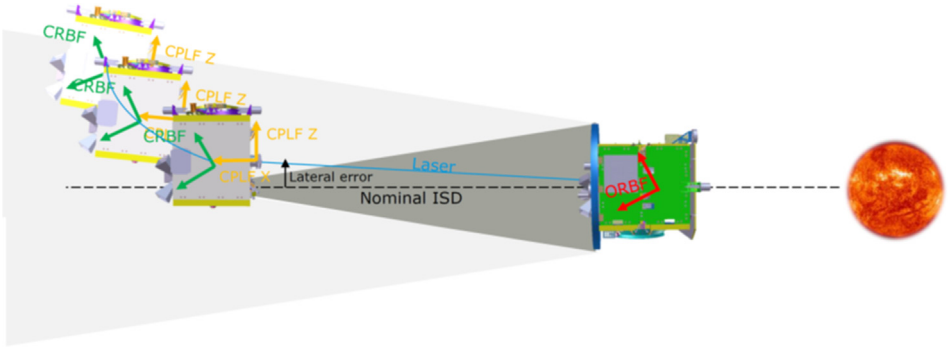

Fig. 6. Position acquisition via metrology control loop (Courtesy of ESA).

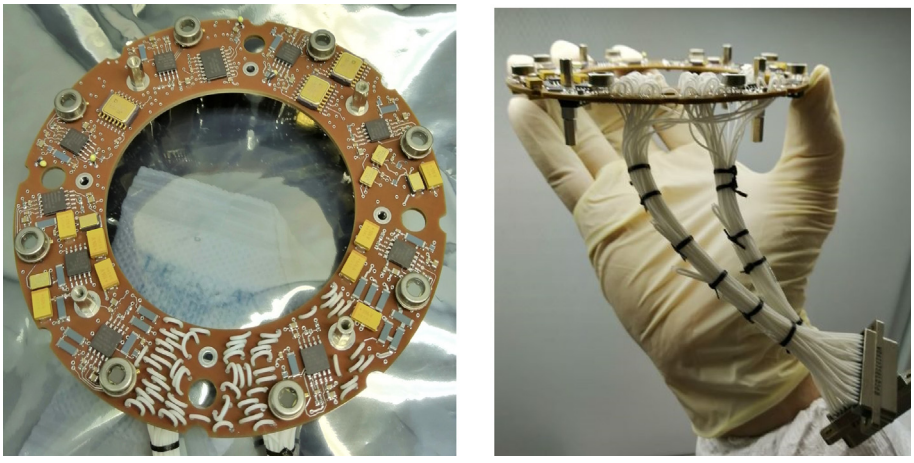

Fig. 7. SPS PCB (engineering model).

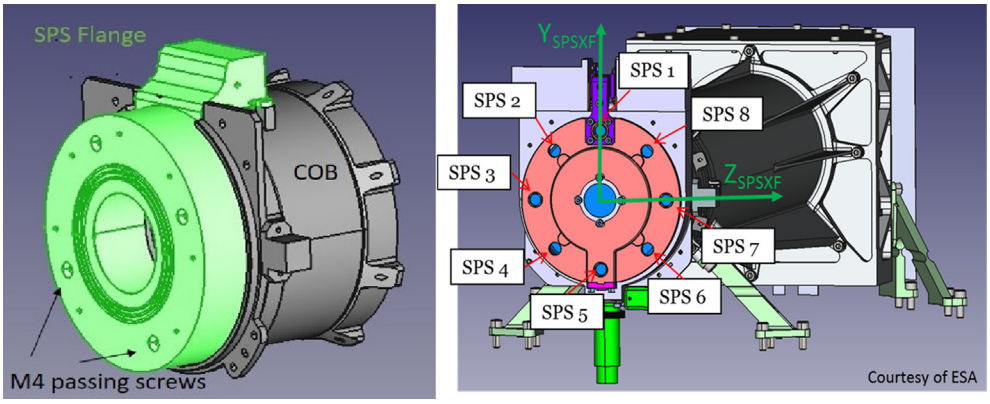

Fig. 8. Left) SPS mechanical flange; Right) SPS diode position referred to the telescope (closed) door.

The SPS PCB is assembled within a toroidal shaped mechanical flange, that is fastened to the Coronagraph Optical Box (COB), as in Fig. 8, left panel. The SPSs look at the deep space and at the Sun toward eight pinholes, with diameter $\varnothing = 2.5$ mm, centred on the SiPM diode and dimensioned to equalize the illuminated area by accounting of the manufacturing and alignment tolerances. A concentric set of teeth constitutes the interface labyrinth with the telescope's Front Door Assembly (FDA) to have contamination control. Fig. 8, right panel, shows the SPS position when covered by the FDA/Lid and their orientation with respect the reference system centred on the Coronagraph's pupil.

The eight SPSs will measure the irradiances in the penumbra generated by the external occulter on the Coronagraph's entrance pupil plane and will monitor the proper

Please cite this article as: D. Loreggia, S. Fineschi, G. Capobianco et al., PROBA-3 mission and the Shadow Position Sensors: Metrology measurement concept and budget, Advances in Space Research, https://doi.org/10.1016/j.asr.2020.07.022

Fig. 9. SPS CAP modified with the insertion of the band pass filters.

positioning by returning the digitized photon budget from opposite sensors (axial symmetry of the penumbra with respect to the entrance pupil). A dedicated metrology algorithm [Casti et al., 2019] will manage these irradiances returning the absolute and relative position of the formation, as described in Section 7.

In order to optimize the diode responsivity and the current-to-voltage conversion (Eq. (3)), the window covering the SPS dye has been modified by gluing a second glass plate, 0.5 mm thick, as shown in Fig. 9, with the internal surface treated with a band pass filter that restricts the observation waveband to the range [500; 650]nm.

The SPS diodes are grouped in two independent sets of four sensors: the nominal set A (1, 3, 5, 7 in Fig. 8, right panel) and the redundant set B (2, 4, 6, 8 in Fig. 8, right panel). During standard operations, in penumbra illumination conditions with the telescope's door open, only the nominal set A will be operated. Moreover, the in-flight optical calibration of the diodes can be done using the only available source that is the Sun. For this reason, the FDA/Lid is designed with holes in front of the SPS pinholes, properly dimensioned to maximize the SPS field of view (and minimize the edge scattering): The four holes in front of the nominal set A house neutral density filters (ND = 2) to observe the Sun without saturation (with the door closed); the four holes in front of the redundant set B are left free to perform measurements during partial eclipse (cross-calibration with nominal set A) and when in penumbra with the door closed [Capobianco et al., 2019].

The SPS is passively powered by the CCB of the coronagraph instrument, that commands the two sets separately. The overall power consumption budget with both the SPS sets on, is of about 2.3 W.

5. SPS measurement concept

As shown in Fig. 10, left panel, the occulting disk projects both a shadow and a penumbra on the Coronagraph's entrance pupil plane. The SPS will measure the photon budget at symmetrical positions, with respect to the pupil centre and, by knowing the theoretical illumination pattern of the penumbra at the given ISD [Bemporad et al., 2015], it will return the position of the CSC with respect to the Sun and to the OSC, i.e. the absolute and relative pointing of the formation. The FF alignment measurement accuracies required to the SPS are:

- 0.5 mm for lateral movements (3σ);
- 50 mm for longitudinal movements (3σ);

within a 3D requirement box of 20x20x200 mm^3, the yellow/smaller volume in Fig. 10, right panel, centred on the nominal FF position. Furthermore, the SPS shall be able to provide the position, without any specified accuracy requirements, over an extended 3D goal box of 100x100x1000 mm^3, the red/larger volume in Fig. 10, right panel.

The measured irradiances are firstly converted in currents and then in voltages by the proximity electronics and amplified by a 2-stage amplification chain [Noce et al., 2019]. Both the outputs of the amplifiers are then digitized by a 12-bit ADC and fed to the Coronagraph Control Box (CCB) by connector wirings and then to the metrology algorithm that is part of the on-board control software, where the measured signals are processed to calculate the FF positioning [Casti et al., 2019]. The SPS will return a position measurement to the GNC with a frequency of 2 Hz.

The algorithm that converts the irradiances into the displacement of the coronagraph with respect to the umbra is based on a proper knowledge of the light distribution on the SPS plane. The photon distribution goes from no illumination for the points in the umbra (no visible fraction of the solar disk) up to total illumination for the points

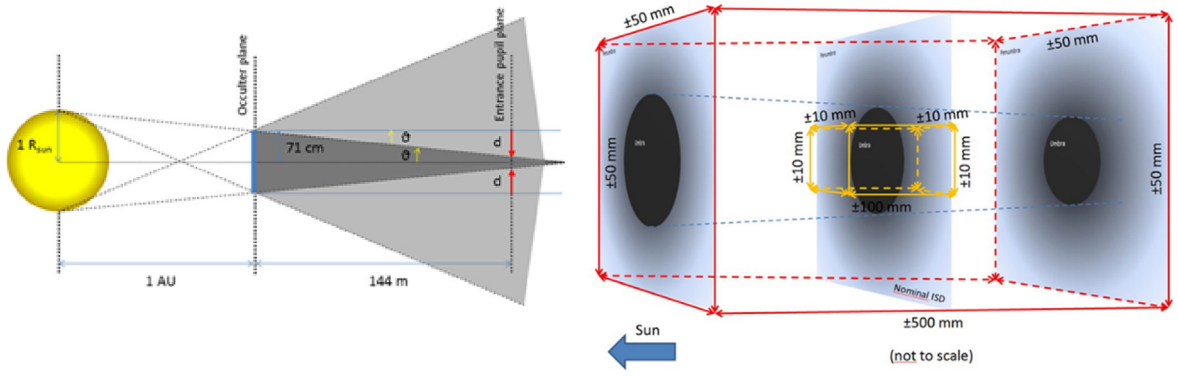

Fig. 10. Cartoon showing: Left) the geometrical penumbral (light grey) and umbra (dark grey) projected by the external occulter on the coronagraph pupil plane; Right) the orientation of the requirement box (yellow/smaller: 20x20x200 mm^3) and of the goal box (red/larger 100x100x1000 mm^3) where SPS measurements should be provided according to mission accuracy requirements. (For interpretation of the references to colour in this figure legend, the reader is referred to the web version of this article.)

Please cite this article as: D. Loreggia, S. Fineschi, G. Capobianco et al., PROBA-3 mission and the Shadow Position Sensors: Metrology measurement concept and budget, Advances in Space Research, https://doi.org/10.1016/j.asr.2020.07.022

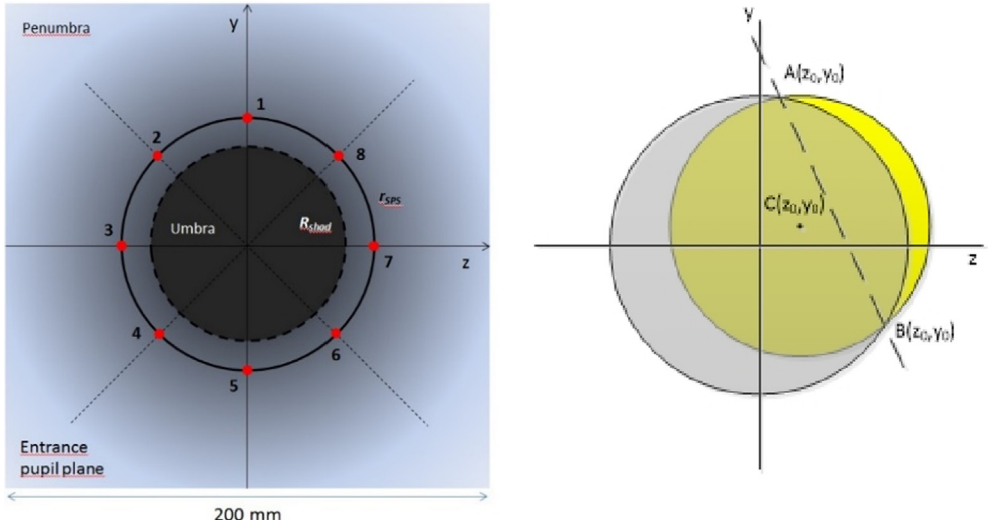

Fig. 11. Left) Simulated umbra and penumbra distribution around the SPS; Right) Cartoon showing the general geometrical configuration defining the location of the solar disk (yellow/decentred filled circle) and the fraction of the disk emerging behind the occulter (grey filled ellipse). (For interpretation of the references to colour in this figure legend, the reader is referred to the web version of this article.)

located out of the penumbra (whole solar disk visible). For all the intermediate points (Fig. 11, left panel) the amount of light coming on a single SPS corresponds to the geometrical area of the Sun crescent not covered by the occulter, as shown in Fig. 11, right panel.

Under the hypothesis to assume a circular shaped solar disk and the occulter edge with an elliptical projected shape (to account of any possible tilt), the derivation of the radiating area seen by the SPS starts from the determination of the intersection points between the circle and the ellipse. Having the ellipse (occulter) centred on the origin of the (y, z) ASPIICS's reference frame with symmetry axes parallel to the main axes of the SPS reference system[1], and the circle (Sun) centre shifted at the position C(y_0, z_0), as in Fig. 11, right panel, the intersection points are given by the solution of the following Eq. 1:

$$\begin{cases} \frac{y^2}{a^2}+\frac{z^2}{b^2}=1 \\ (y-y_0)^2+(z-z_0)^2=R^2 \end{cases} \rightarrow \alpha y^4+\beta y^3+\gamma y^2+\delta y+\varepsilon=0 \tag{1}$$

From the intersection points, and knowing the angular dimensions of the Sun and of the occulter disk, and the spectral intensity of the Sun, we can obtain the radiating area by integrating the radiance with the following constraints: a) the Sun is not a perfect circle; b) the occulter projection can vary within mission requirements; c) the illumination of the Sun is not uniform over the disk, because of the limb darkening effect [Cox, 2000]; d) the waveband of operation of the SPS [500;650]nm; e) the spatial filtering due to the pinholes dimensions $\varnothing = 2.5$ mm that univocally define the acceptance solid angle Ω_{SPS}.

Finally, we have that the irradiance L at the SPS level (Eq. 2) is:

$$L=\int_{A_{pinhole}}\int_{\Omega_{SPS}} \times \int_{\lambda_{min}}^{\lambda_{max}} I_\lambda\left(1-u_\lambda-v_\lambda+u_\lambda cos\vartheta+v_\lambda cos^2\vartheta\right)d\lambda\, d\omega\, dy\, dz \tag{2}$$

where u_λ, v_λ are the limb darkening coefficients [Cox, 2000] and I_λ is the spectral intensity.

6. SPS transfer function

The SPS diodes convert the irradiance L in current via the relation $C_{SPS} = K^{-1} \cdot L$ where the factor K^{-1} is the "diode effective responsivity" that accounts for the spectral flux F_λ, the transmissivities of the diode protection window T_W, and of the applied band pass coating T_F, and for the SiPM quantum efficiency at the operation waveband and temperature, $\varepsilon_{SPS}(\lambda, T_{SPS})$. The K factor has units of [W/A] and is defined as [Bemporad et al., 2015]:

$$K=\frac{\int_{A_{\text{pinhole}}}\int_{\Omega_{SPS}}\int_{\lambda_{\min}}^{\lambda_{\max}} I_{\lambda 0}(1-u_\lambda-v_\lambda+u_\lambda\cos\vartheta+v_\lambda\cos^2\vartheta)d\lambda d\omega dydz}{\int_{A_{\text{pinhole}}} f_{\text{SPS}}\frac{\langle G(\vartheta)\rangle_{\Omega_{SPS}}}{\langle G(\vartheta)\rangle_{\Omega_s}}\int_{\lambda_{\min}}^{\lambda_{\max}} F_\lambda T_W(\lambda)T_F(\lambda)\varepsilon_{SPS}(\lambda,T_{SPS})d\lambda dydz} \tag{3}$$

f_{SPS} is the fraction of Sun disk seen by the SPS.

In the considered waveband, the effective responsivity K^{-1} is weakly dependent on the position across the penumbra profile and it can be assumed constant (this being the

[1] The coordinate axes for ASPIICS/PROBA-3 are oriented such that the x-axis is along the optical axis, pointing to the ASPIICS detector, the y-axis is along the vertical to the coronagraph optical bench and the z-axis complete the right-handed triad. The (y,z) orthogonal plane is assumed centered on the telescope's entrance pupil.

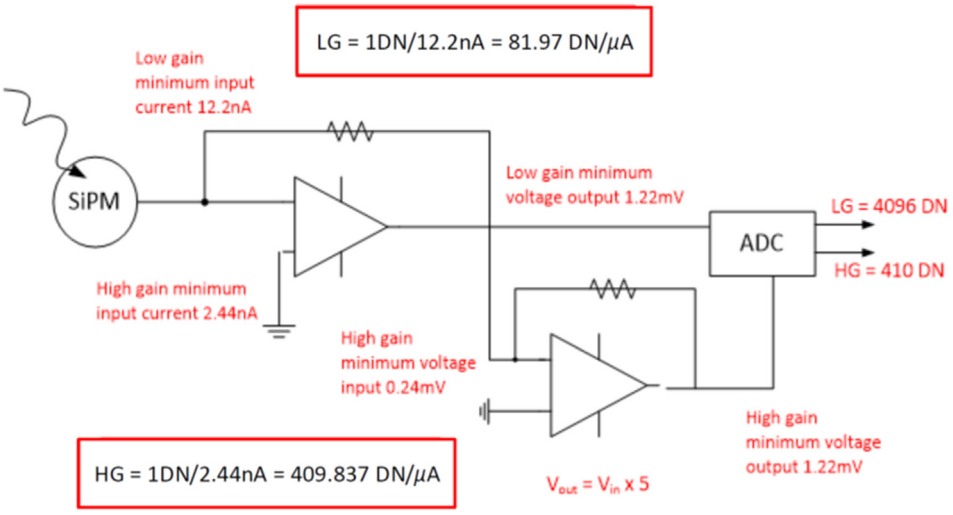

Fig. 12. SPS electronics amplification chain.

main reason for filtering). The current C_{SPS} generated from each sensor is transformed in a voltage by a *trans*-impedance amplification stage as V_{TIA} [mV] = A_{TIA}[kΩ] · C_{sps} [μA], where A_{TIA}(kΩ) is the *trans*-impedance amplification factor.

Within the volume of relative spacecraft displacements, the Sun irradiance shows a huge variation. In order to have the proper sensitivity over the full dynamic range, the proximity electronic has been designed adopting two-gain amplification chains: Low Gain (LG) (that corresponds to the A_{TIA}) and the High Gain (HG), with a constant ratio HG/LG = 5 as schemed in Fig. 12. LG measurements are used to cover the illumination full range and the HG measurement to return the expected accuracy in low light conditions.

The amplified voltages are then digitized by the 12-bit ADC and fed to the CCB by connector wirings. Here, the SPS digitized readouts are processed by the SPS metrology algorithm embedded in the OBSW. As a first step, the HG measurement is compared with a reference threshold such that when HG < 4000 DN, namely in low light regime, it is retained for the position calculation otherwise it is discarded and the LG output is used.

In this latter case, before final processing of the signal, the LG readouts are multiplied by 5 to have the proper continuity with the HG values and to have the correct mapping of the displacements range.

7. SPS metrology algorithm

The SPS metrology algorithm receives in input both LG and HG measurements of the penumbra profile and returns the position measurement to the GNC loop, after having applied different calculation procedures.

The four readouts from the nominal set A and the four readouts from the redundant set B are considered, separately. The algorithm will be informed on what set is working (in nominal condition only set A is operated) and the corresponding digitized LG or HG amplified irradiances are used to retrieve the FF positioning. To this aim, four different procedures are run: three procedures calculate the FF misalignment on the lateral plane (y, z), orthogonal to the optical axis of the coronagraph, and centred on the entrance pupil; the fourth routine computes the longitudinal coordinate x, using in input the (y, z) coordinates retrieved by the previous ones.

The best strategy for the computation of the relative position will be identified during FF operation on the base of data on-ground post-processing.

The estimated position is returned with several validity flags that inform the control system about the effectiveness of the SPS measurements, taking into account: the flux regime, the proximity temperature, the relative drift of the two satellites, and any possible noise that could somehow make the SPS measurements not valid [Casti et al., 2019].

In the following subsections, the procedures for the position calculation are listed and described in order of complexity.

7.1. Lateral positioning

- The *differential algorithm*: it provides qualitative response about the satellites alignment, determining whether the two spacecraft are in the aligned configuration or not, and providing a rough estimate of the misalignment direction at a given time. In order to minimize any possible uncertainty related to the radiometric calibration of each SPS, the differential algorithm computes relative and not absolute differences as given in Eq. (4).

Please cite this article as: D. Loreggia, S. Fineschi, G. Capobianco et al., PROBA-3 mission and the Shadow Position Sensors: Metrology measurement concept and budget, Advances in Space Research, https://doi.org/10.1016/j.asr.2020.07.022

$$\delta_{15} = \frac{R_1 - R_5}{R_1 + R_5}; \quad \delta_{37} = \frac{R_3 - R_7}{R_3 + R_7}; \quad \delta_{26} = \frac{R_2 - R_6}{R_2 + R_6}; \quad \delta_{48} = \frac{R_4 - R_8}{R_4 + R_8} \tag{4}$$

This algorithm will be extremely useful during the in-flight calibration, when it will be necessary to perform a fine-tuning of the parameters used by the others procedures (e.g., the pseudo-paraboloid fitting parameters).

- The *linear algorithm*: it gives a first quantitative estimation of the occulter position on the (y,z) plane. As the differential algorithm, it is based on the difference of signals measured by opposite SPSs but implies to have the in-flight calibration of the irradiance profile in order to retrieve absolute measurements, as in Eq. 5:

$$z_0 = \frac{R_3 - R_7}{d}; \quad y_0 = \frac{R_1 - R_5}{d} \tag{5}$$

where d is a calibration coefficient that accounts of the reference nominal FF position.

- The *pseudo-paraboloid algorithm:* it is the most complex one and it is based on a third order polynomial fitting of the computed penumbra profile generated by the occulter. If we indicate with R the reading at each SPS location, the best fit of the penumbra is returned as:

$$R = \frac{|z - z_0| + |y - y_0|}{a} + \frac{(z - z_0)^2 + (y - y_0)^2}{b^2} + \frac{|z - z_0|^3 + |y - y_0|^3}{c^3} + R_0 \tag{6}$$

where *a, b, c*, are the fitting coefficients, and R_0 is a variable related to the longitudinal position x_0 calculated as the average of the four radiance values returned by the four SPSs at the nominal ISD [Bemporad et al., 2015]. Applying Eq. (6) to each SPS (Fig. 11, left panel), and solving for y_0 and z_0, after some mathematics, the resulting equations Eq. 7 and Eq. 8 providing the occulter centre position are [Bemporad et al., 2015]:

$$y_0 = 2\sqrt{-A/3}\cos\left\{\frac{1}{3}\left[\cos^{-1}\left(\frac{(R_5 - R_1)c^3}{4\sqrt{-(A/3)^3}}\right) + 4\pi\right]\right\}$$
$$z_0 = 2\sqrt{-A/3}\cos\left\{\frac{1}{3}\left[\cos^{-1}\left(\frac{(R_3 - R_7)c^3}{4\sqrt{-(A/3)^3}}\right) + 4\pi\right]\right\} \tag{7}$$

with:

$$A = c^3\left(\frac{1}{a} + \frac{2r_{SPS}}{b^2} + \frac{3r_{SPS}^2}{c^3}\right) \tag{8}$$

With r_{SPS} = 55 mm the radial position of the SPS respect to the centre of the reference system centred on the ASPIICS's entrance pupil.

7.2. Longitudinal positioning

Once obtained the lateral position, the longitudinal position x is calculated by finding the solution of the second order polynomial that has been found being the best fitting approximation (at first order) to represent the evolution of the SPS lateral measurement along the longitudinal direction. If we refer to the simulated SPS counts at the radial distance of 55 mm from the centre of the umbra as $R_{55}(x_0)$, the variation of the penumbra irradiance along the x coordinate can be fitted by a quadratic function, as:

$$R_{55} = Hx^2 + Kx + L \tag{9}$$

The main assumption for the application of this method to the calculation of the longitudinal coordinate is that the shape of the pseudo-paraboloid representing the penumbra distribution on the plane orthogonal to the optical axis is preserved for any displacement dx. This is not exactly true but we verified that it is an acceptable approximation giving a residual error within the accuracy specification, as shown in the following section. We obtain the x_0 coordinate, as:

$$x_0 = \frac{-K - \sqrt{K^2 - 4H(L - R_{55comp})}}{2H} + \frac{1}{4}d_0^2 \tag{10}$$

where $d_0^2 = y_0^2 + z_0^2$, and H, K, L are the coefficients of the parabolic fitting curve (calculated at the nominal ISD). $R_{55\text{-}comp}$ represents the discrepancy between the measured values and those referred to the aligned FF [Casti et al., 2019].

8. Algorithm performances test

We tested the algorithm running the different procedures for a set of simulated SPS measurements, representative of different spacecraft relative and absolute positions.

A matrix representation of the digitalized penumbra profile, as returned by the system electronics, was generated, covering a 2D space of 130mm × 130mm, divided in squares of 10μm × 10μm. The centre of this area corresponds to the centre of the umbra, which is also the occulter geometrical centre.

Assuming, as still remarked, that moving along the longitudinal direction the shape of the penumbra profile does not change, a 3D volume of 2D matrices was built for a set of longitudinal FF misalignments so to obtain a 3D box as more as possible representative of the yellow/smaller box shown in Fig. 10, left panel, compatibly with the calculation time consumption.

The algorithm has been implemented in Matlab code and tested with reference values of the various fitting parameters as returned by the penumbra profile simulation at the reference ISD. The main assumption for the fitting procedure is to consider two different sets of coefficients: one set for a coarse fit, used for lateral positioning far from the FF nominal position; a second set for a fine fit, used for lateral positioning around to the nominal position.

It has been shown that the best results are obtained when the boundary between the region of validity for the two fitting solutions is fixed at 13.8 mm. When a lateral displacement of the FF is lower than this limit, the best estimation is returned by applying the fine fit; when the

Please cite this article as: D. Loreggia, S. Fineschi, G. Capobianco et al., PROBA-3 mission and the Shadow Position Sensors: Metrology measurement concept and budget, Advances in Space Research, https://doi.org/10.1016/j.asr.2020.07.022

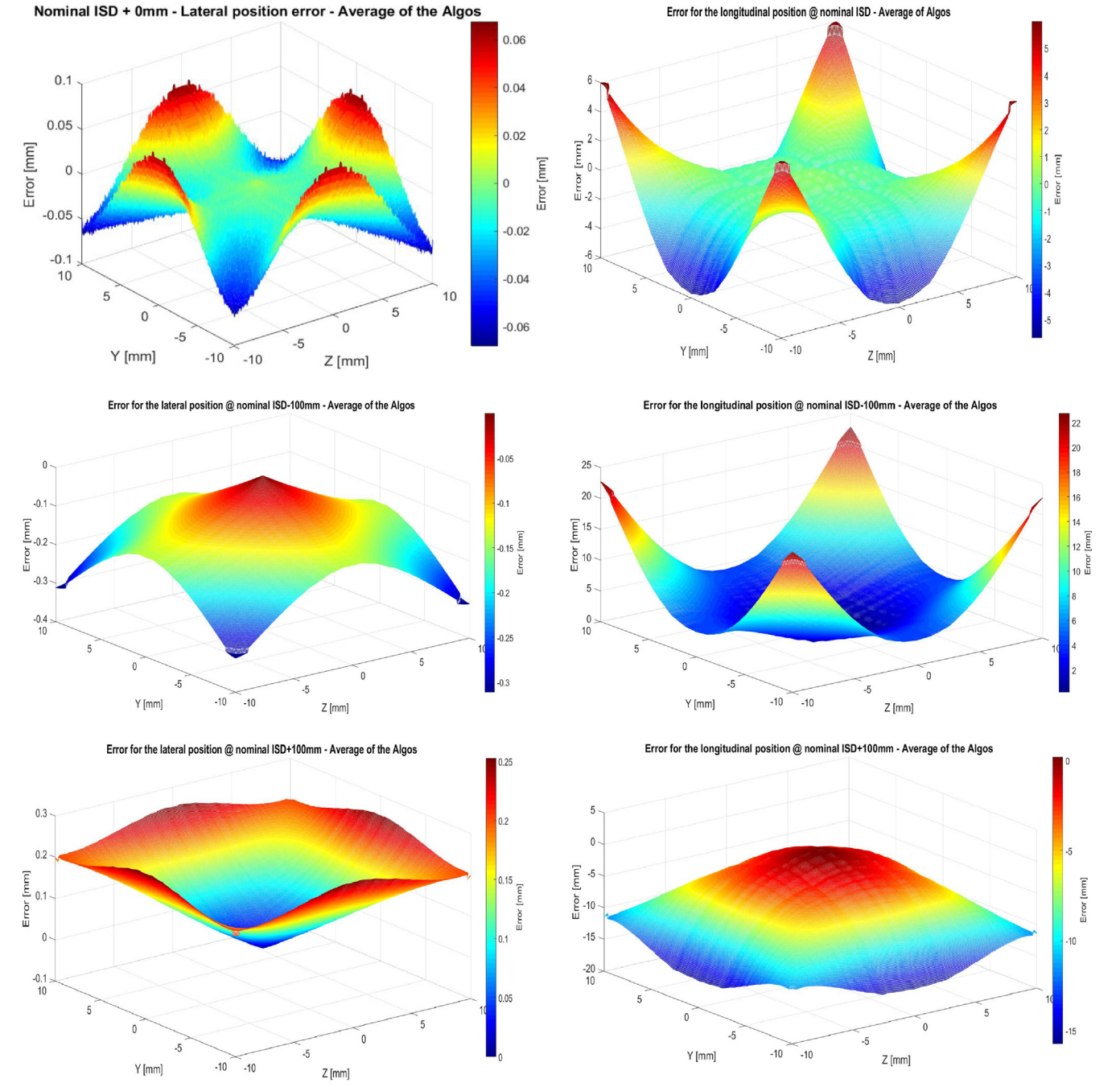

Fig. 13. SPS measurement error map obtained from simulations at nominal ISD, ISD-100 mm and ISD + 100 mm (requirement box): Left) lateral; Right) longitudinal.

displacement is larger, the best solution is returned by the coarse fit.

The algorithm performances have been verified assuming a known misalignment and giving in input to the SPS the corresponding expected irradiance values, obtained by mapping the penumbra profile. The difference between the values calculated by the algorithm and the considered displacement quantifies the implicit algorithm error. During verification and testing of the metrology algorithm, we found that the performances improve when the result of the pseudo-paraboloid fitting procedure is combined with the result of the linear procedure (average of position estimations). In Fig. 13, the resulting error distribution for lateral (left) and longitudinal (right) misalignment, are given.

The error map was obtained computing the occulter centre position varying within the requirement box (yellow/smaller in Fig. 10, right) and combining the outcomes of both linear and pseudo-paraboloid algorithms. As it is possible to observe, the maximum absolute lateral error at the nominal ISD is about 60 μm, while the worst case at the longitudinal extremes of the requirement box is 250 μm.

Please cite this article as: D. Loreggia, S. Fineschi, G. Capobianco et al., PROBA-3 mission and the Shadow Position Sensors: Metrology measurement concept and budget, Advances in Space Research, https://doi.org/10.1016/j.asr.2020.07.022

Table 4
SPS error budget.

Contribution	Lateral (μm)	Longitudinal (mm)
Metrology System Error Budget		
Readout electronics	1	0.2
Algorithms – Fit of penumbra profile (worst case)	250	20
Ageing + radiation (EOL without periodical calibration)	160	32
In-flight calibration residuals (3-months periodicity)	21	4.2
On-ground calibration residuals	5	1
Uncertainties on the Penumbra Illumination Profile		
Diffraction	600	120
Sunspots**	160	8
Total		
EOL (End of Life) without penumbra assessment and only initial calibration	897	158
EOL with penumbra assessment and periodical calibrations	251	20

** These are occasional events with additive contribution.

The longitudinal error map was obtained considering a lateral relative movement of the two spacecraft at different ISD (nominal, nominal ± 100 mm) and verifying the capability of the paraboloid approximation, Eqs. (9) and (10), to return the longitudinal position. The maximum error is about 20 mm.

Both lateral and longitudinal errors are well within the SPS accuracy requirements.

9. SPS error budget

In Table 4, we give the error budget of the full measurement chain, accounting of the photon noise, the electronic contribution, the algorithm, the calibration residuals, and the uncertainty in the penumbra knowledge.

The largest contribution to the error comes from the unknowledge of the real penumbra profile that is the sum of the geometric irradiance distribution behind the occulter and of the diffraction generated by the occulter. Physical random events, such as sunspots, can also significantly reduce the measurement accuracy (even if for small periods). The metrology algorithm implements several evaluation steps to verify when a positioning measurement can be considered valid or not, so that, as still underlined, each SPS readout is flagged to inform the OBSW about the effectiveness of the reading. Periodic in-flight calibration plays a critical role to satisfy the EOL accuracy requirements [Capobianco et al., 2019].

10. SPS status

The SPS program completed the qualification campaign with the delivery of the Engineering Qualification Model – EQM. The SPS flange has been internally finished with ACKTAR Magic Black to minimize any spurious light that could disturb the SPS measurements (Fig. 14a and b). The inner surface of the SPS that is part of the ASPIICS telescope tube has been also blackened to control stray light toward internal optics.

The front surface, facing the deep space and the Sun, has been finished with MAP-PCBE silicon white paint to optimize thermal properties (Fig. 15). All other external surfaces have been treated with Alodine1200 to protect against corrosion. Fig. 15 shows the SPS assembled and mounted over a supporting fixture used for thermal testing. The EQM PCB, shown in Fig. 7, is assembled inside the flange and the connectors properly mounted in order to exit the holes on the connector bracket (shown in

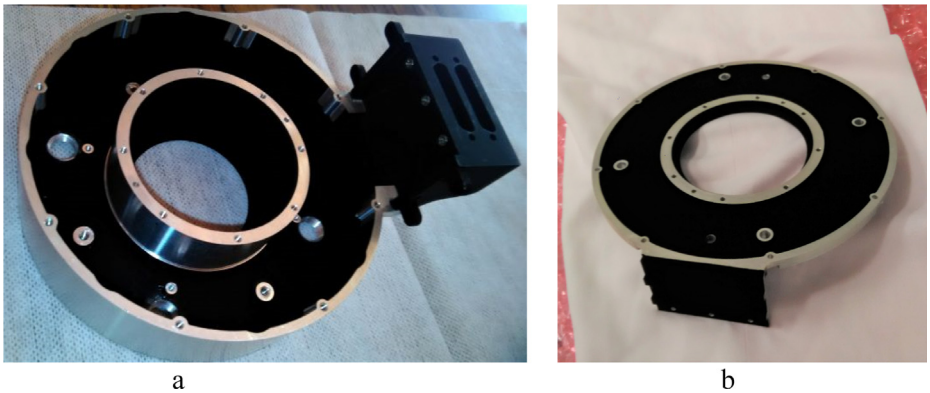

a b

Fig. 14. EQM SPS flange: Inside view before assembly.

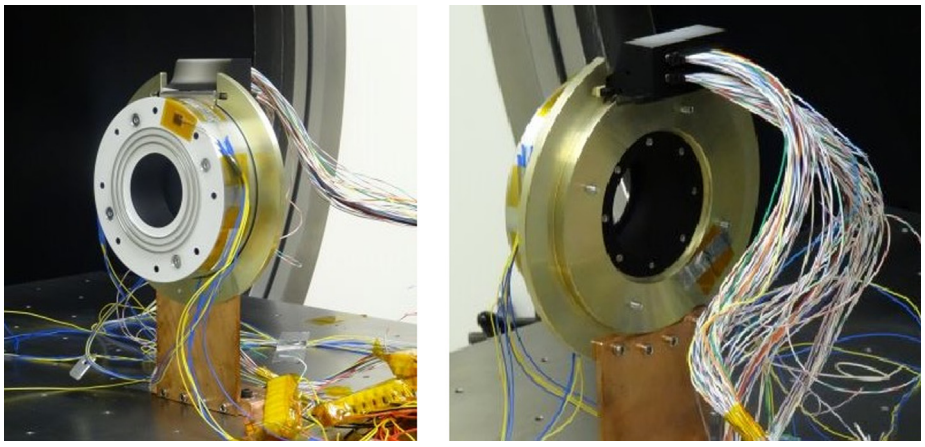

Fig. 15. EQM SPS assembled with the PCB: Connectors properly mounted to have external link to the control unit.

Fig. 14a). The cabling to the electronic ground segment equipment (EGSE), used for verification of the SPS functionalities during the qualification phases, is also shown.

The production of the SPS flight model (FM) started at the beginning of 2020, and the final delivery is currently expected for end of 2020.

11. Conclusions

We present a review of the PROBA-3 mission of the European Space Agency, a cornerstone technological mission aimed at in-orbit validation of different metrology sub-systems and control algorithms for a two-spacecraft formation flying. At the end of the two years mission, PROBA-3 is expected to return a complete robust autonomous formation flying architecture including GNC validation, and formation safety and repeatability manoeuvres configurations. Moreover, being the validation tool a diluted coronagraph, with the telescope on one spacecraft (CSC), named ASPIICS, and the occulter on the other one (OSC), at inter-satellite distance of 144.3 m, scientifically relevant coronagraphic observations at high spatial and temporal resolution down to $1.08R_{Sun}$ will be provided.

Between the metrology sub-systems, the Shadow Position Sensors (SPS), a series of 8 SiPM disposed around the ASPIICS's entrance aperture, is the active most critical one. It aims at measuring the proper centring of the penumbra projected by the external occulter with the centre of the coronagraph entrance pupil, with sub-millimetre accuracy. Starting from the irradiance measurements, that in FF conditions will be the same on each sensor, the monitoring of any variation from the symmetry condition will permit to calculate, by mean of a dedicated metrology algorithm, the lateral and longitudinal misalignment of the two spacecraft, and to return to the GNC the information for the relative and absolution re-alignment of the formation. In this paper, we describe the SPS system architecture, the measurement concept, and the metrology algorithm showing how the expected performances are in agreement with the mission accuracy requirements. The status of the SPS program is finally outlined.

Declaration of Competing Interest

The authors declare that they have no known competing financial interests or personal relationships that could have appeared to influence the work reported in this paper.

Acknowledgments

The authors acknowledge the support provided by the PROBA-3 Managerial and Technical Staff of the European Space Agency (ESA) within the contract with the Centre Spatial de Liège (CSL) and subcontractors, subscribed for the Payload Instrument design and development (C/D Phases).

References

Baccani, C., Landini, F., Romoli, M., et al., 2016, Preliminary evaluation of the diffraction behind the PROBA 3/ASPIICS optimized occulter. In: MacEwen, H.A., Fazio, G.G., Lystrup, M. (Eds.). Proc. of SPIE Space Telescopes and Instrumentation, Vol. 9904, Optical, Infrared, and Millimeter Wave, 990450. Edinburgh, UK. https://doi.org/10.1117/12.2232534.

Bemporad, A., Baccani, C., Capobianco, G., et al., 2015, The Shadow Positioning Sensors (SPS) for formation flying metrology on-board the ESA-PROBA3 mission. In: Fineschi, S., Fennelly, J. (Eds.) Proc. of SPIE Optical Engineering and Applications, Vol. 9604, Solar Physics and Space Weather Instrumentation, 96040C; San Diego, CA, US. https://doi.org/10.1117/12_2191829.

Blackwood, G.H., Serabyn, E., Dubovitsky, S., et. al., 2003, System design and technology development for the Terrestrial Planet Finder infrared interferometer. In: Coulter, D.R. (Ed.) Proc. SPIE Optical Science and Technology, Vol .5170, Techniques and Instrumentation for Detection of Exoplanets. Bellingham, WA. San Diego, CA, US, pp. 129-143. https://doi.org/10.1117/12.521311.

Bodin, P., Larsson, R., Nilsson, F., Chasset, C., Noteborn, R., Nylund, M., 2009. PRISMA: An In-Orbit Test Bed for Guidance, Navigation, and Control Experiments. J. Spacecraft Rockets 46 (3), 615–623, Published by American Institute of Aeronautics and Astronautics, Inc..

Capobianco, G., Fineschi, S., Loreggia, D., et al., 2019, The in-flight calibration of the shadow position sensors, optical metrology system of

the ESA/PROBA-3 formation flying mission. In: Presentation at International Workshop on Satellite Constellation and Formation Flying; Glasgow, UK.

Casti, M., Bemporad, A., Fineschi, S., et al., 2019, PROBA-3 formation-flying metrology: algorithms for the shadow position sensor system. In: Sodnik, Z., Karafolas, N., Cugny, B., Chania, G.R. (Ed.), Proc. of the International Conference on Space Optics — ICSO 2018, Vol. 11180. p. 82. https://doi.org/10.1117/12.2536209.

Contreras, R., Penin, L.F., Marco, V., et al., 2017, PROBA-3: High Precision Formation Flying in HEO, Advances in the Astronautical Sciences Guidance, Navigation and Control, Vol. 159, AAS 17-094; Edited by R. R. Rohrschneider; Breckenridge, CO, US;

Covello, F., Battazza, F., Coletta, A. et al., 2008. COSMO-SkyMed mission status. In: Bruzzone, L., Notarnicola, C., Posa, F. (Eds.) Proc. SPIE Remote Sensing, Vol. 7109, Image and Signal Processing for Remote Sensing XIV, 710918. Cardiff, UK. https://doi.org/10.1117/12.803731.

Cox, A.N. 2000, Allen's astrophysical quantities. In: Arthur N. Cox, (Ed.), AIP Press; Springer, NY, US.

Escoubet, C., Schmidt, R. & Goldstein, M., 1997, CLUSTER – Science and Mission Overview, Space Science Reviews 79. Kluwer Academic Publishers, BE, pp.11–32. https://doi.org/10.1023/A:1004923124586.

Galano, D., Jollet, D., Mellab, K., et al., 2019, PROBA-3 formation flying mission, Presentation at the International Workshop on Satellite Constellation and Formation Flying, IWSCFF 19-37, Glasgow, UK.

Galy, C., Fineschi, S., Galano, D., et al., 2015, Design and Modelisation of ASPIICS Optics. In: Fineschi, S., Fennelly, J. (Eds.). Proc. of SPIE Optical Engineering and Applications, Vol. 9604, Solar Physics and Space Weather Instrumentation VI, 96040B. San Diego, CA, US. https://doi.org/10.1117/12.2188404.

Glassman, T., Lo, A.S., Arenberg, J., et al., 2009, Starshade scaling relations. In: Shaklan, S.B. (Ed.). Proc of SPIE Optical Engineering and Applications, Vol. 7440, Techniques and Instrumentation for Detection of Exoplanets IV, 744013. San Diego, CA, US, https://doi.org/10.1117/12.825033.

Jennrich, O., 2004, LISA: a mission to detect and observe gravitational waves. In: Hough, J., Sanders, G.H. (Eds.). Proc. of SPIE Astronomical Telescope and Instrumentation, Vol. 5500, Gravitational Wave and Particle Astrophysics Detectors. Glasgow, UK, pp. 113–119. https://doi.org/10.1117/12.554917.

Landgraf, M., Mestreau-Garreaub, A., 2013. Formation flying and mission design for PROBA-3. Acta Astronautica 82 (1), 137–145. https://doi.org/10.1016/j.actaastro.2012.03.028, Edited by Elsevier.

Leitner, J., 2004, Formation Flying – The future of remote sensing from space. In: International Symposium on Space Flight Dynamics (ESA SP-548), Munich, DE.

Krieger, G., Moreira, A., Fiedler, H., et al., 2007, TanDEM-X: A Satellite Formation for High-Resolution SAR Interferometry in IEEE Transactions on Geoscience and Remote Sensing, Vol. 45, no. 11, pp. 3317-3341; Edited by IEEE; doi: 10.1109/TGRS.2007.900693;

Noce, V., Loreggia, D., Belluso, M., et al., 2019. Metrology on-board PROBA-3: the shadow position sensors subsystem. In: Presentation at the International Workshop on Satellite Constellation and Formation Flying, Glasgow, UK.

Tapley, B.D., Bettadpur, S., Watkins, M., Reigber, C., 2004. The Gravity Recovery and Climate Experiment: Mission overview and early results. Geophys. Res. Lett. 31 (9), 4. https://doi.org/10.1029/2004GL019920, Edited by American Geophysical Union.

Xiang, W., Jorgensen J.L., 2005, Formation Flying: A subject being fast unfolding in space. In: 5th IAA Symposium on Small Satellites for Earth Observation; Berlin, DE.

Wallner, O., Ergenzinger, K., Flatscher, R., Johann, U., 2006, DARWIN mission and configuration trade-off. In: Monnier, J.D., Schöller, M., Danch, W.C. (Eds.). Proc. of SPIE Astronomical Telescopes and Instrumentation, Vol. 6268, Advances in Stellar Interferometry; 626827. Orlando, FL; US. https://doi.org/10.1117/12.671658.

Werninghaus, Rolf., 2004, TerraSAR-X mission. In: Posa, F. (Ed.), Proc. of SPIE Remote Sensing, Vol. 5236, SAR Image Analysis, Modeling, and Techniques VI. Barcelona, SP, pp. 9-16. https://doi.org/10.1117/12.511500.

Zuckov, A., 2018, The PROBA-3 mission and its contribution to the studies of the magnetic field in the solar corona. In: 42nd Presentation at COSPAR Scientific Assembly, Pasadena, CA, US.

Please cite this article as: D. Loreggia, S. Fineschi, G. Capobianco et al., PROBA-3 mission and the Shadow Position Sensors: Metrology measurement concept and budget, Advances in Space Research, https://doi.org/10.1016/j.asr.2020.07.022

View publication stats